Return Current in Large Aperture Electron-Beam Excited KrF Lasers

MARK J. KUSHNER, SENIOR MEMBER, IEEE

Abstract—**In electron-beam (e-beam) excited lasers, the charge injected into the laser chamber must return to the grounded walls. The electric potential generated by the injected charge drives the return current to the walls, and results in joule heating of the plasma. In large aperture inertial confinement fusion class e-beam excited lasers (aperture size > 1 m) the spatial redistribution of power deposition caused by the return currents is a nonneglible fraction of the total, particularly near the foils where power deposition by the e-beam is low. In these cases, the e-beam excited laser functionally operates as an e-beam sustained discharge. In this paper, results from a model for an e-beam excited KrF laser are presented, and the effects of return currents on plasma parameters and laser performance are discussed. We find that the joule heating caused by the return currents, expressed as a fraction of total power deposition, increases with increasing halogen density, increasing aperture size, increasing pressure, and decreasing power deposition. The return current electric field causes a decrease in the rate coefficients for dissociative recombination and attachment, and an increase in the rate of multistep ionization. As a result the electron density near the foil increases by >10's %. The laser intensity in those regions also increases. These effects are practically important in lasers having apertures exceeding 1 m.**

I. INTRODUCTION

ELECTRON-beam (e-beam) excitation is a common method of pumping large aperture gas lasers, and excimer lasers in particular [1]–[5]. In e-beam excited lasers, the charge deposited in the gas by the beam must return to the walls of the chamber which serve as the electrical ground [6]. To drive the return current $\vec{j}_r$ the injected charge generates an electrical potential $\phi_r(\vec{r})$ within the chamber. The return current electric field due to this potential $\vec{E}_r(\vec{r})$ results in joule heating of the medium $\vec{j}_r \cdot \vec{E}_r$. Conceptually, the power deposited by this joule heating comes from the potential energy gained by the beam electrons which previously climbed the potential hill represented by ϕ_r. The joule heating caused by the return currents can therefore be thought of as a redistribution of a portion of the kinetic energy carried by the beam electrons into the chamber. By appropriate choices of e-beam parameters, gas pressure, and geometry one can capitalize on the return current heating to provide the primary pumping of the gas, as has been demonstrated by Mangano *et al.* [6] for a KrF laser.

Manuscript received December 1, 1989; revised February 23, 1990. This work was supported by Los Alamos National Laboratory and by the National Science Foundation under Grants ECS 88-15781 and CBT 88-03170.

The author is with the Department of Electrical and Computer Engineering, University of Illinois, Urbana, IL 61801.

IEEE Log Number 9037370.

The presence of $\vec{E}_r$, and its resulting joule heating, impacts the operation of an e-beam excited laser in at least two ways. First, the portion of power deposition redistributed as joule heating by the return current may be a nonneglible fraction of the total power deposited by the beam electrons. The spatial profile of power deposition may therefore be affected. The spatial distribution of processes whose rates depend on power deposition, such as formation of the upper laser level in excimer systems, will also therefore change. Second, even if joule heating by the return current is not significant, the electron energy distribution (EED) of the low-temperature "bulk" electrons may be altered by $\vec{E}_r$. This effect will alter electron impact rate coefficients which have low threshold energies such as dissociative attachment to, for example, F_2 in gas mixtures used for KrF lasers.

The magnitude of $\vec{E}_r$ can be quickly estimated from [6]

$$j_b = \frac{PL}{V_b} = e n_e \mu_e E_r \tag{1}$$

where j_b is the current density of the electron beam, P (W-cm^{-3}) is the average power deposited by the beam, L is the transverse dimension of the chamber, V_b is the electron beam voltage, n_e is the bulk electron density, and μ_e is the bulk electron mobility. We have assumed that all of the beam energy is deposited in the gas. Equation (1) is simply an equality between the injected current density and that driven by the return current field back to ground. In attachment dominated plasmas, as used for KrF excimer lasers having F_2 as the halogen donor, the bulk electron density can be estimated by

$$n_e \approx \frac{P}{W[\mathrm{F_2}]k_a} \tag{2}$$

where W is the "W value" value for ionization [7] by beam electrons, and k_a (cm^3-s^{-1}) is the electron impact rate coefficient for attachment. Since $\mu_e = e/(m_e \nu_m)$, where ν_m is the collision frequency for momentum transfer and $\nu_m = k_m \cdot N$ (k_m is the rate coefficient for momentum transfer), we have

$$E_r/N \approx \left(\frac{W m_e k_a k_m}{e^2}\right) \cdot \left(\frac{[\mathrm{F_2}]L}{V_b}\right). \tag{3}$$

Here we have expressed the return current electric field as E_r–N, where N is the gas density, since this is the common scaling parameter for excitation rates in electric dis-

charge excited plasmas [9]. In (3), k_a and k_m may be functions of E_r–N and the gas mixture, while W is a function only of gas mixture. The first grouping of terms are fundamental values of the gas mixture which cannot be externally adjusted. The terms in the second group can be selected by the operator. E_r–N increases with increasing fluorine density since the electron density scales as $1/[F_2]$. A lower electron density requires a larger electric field to obtain a given current density and to convect a given amount of charge out of the chamber. E_r–N increases with increasing chamber dimensions since for a given $P(\text{W-cm}^{-3})$ there is more charge to convect back to the walls with increasing L. Finally, E_r–N decreases with increasing V_b (for constant power deposition) since as V_b increases a lower beam current is required to maintain a fixed value of P. As discussed below, the return current electric field is most sensitive to the gas mixture and size of the chamber.

Using values typical of e-beam excited KrF lasers, we find that $0.1\ \text{Td} \leq E_r\text{–}N \leq 3\ \text{Td}$, where $1\ \text{Td} = 1 \cdot 10^{-17}$ V-cm^{-2}. In an e-beam excited plasma, as used for a KrF laser, the electron temperature is $T_e \approx 1.5$ eV [8]. In a discharge using the same gas mixture, this temperature is obtained with an applied electric field of 3–6 Td. Therefore one might expect that the return currents in an e-beam excited laser are large enough to heat the bulk electrons and therefore perturb the bulk electron energy distribution. In this respect, large e-beam excited lasers resemble e-beam sustained discharges. Observations of "hot spots" on the foils of e-beam pumped lasers may be the result of this discharge-like behavior [10]. The change in the plasma potential caused by E_r can be estimated by integrating E_r across $L/2$. Doing so, we find that in large aperture lasers ($L \geq 10$'s cm) using multiatmosphere gas mixtures, ϕ_R can approach 10's of kV, a value that could also perturb the trajectories and slowing down of beam electrons.

In this paper, the effects of return currents on fusion class e-beam excited KrF lasers ($L \geq 1$ m) are investigated. This investigation is performed with the results from a three-dimensional Monte Carlo simulation for electron beam power deposition, a Boltzmann analysis for the bulk electron energy distribution (EED), and a one-dimensional plasma chemistry model for the KrF laser. We will find that the effects of return currents on power deposition and plasma kinetics are greatest near the walls of the chamber. This results from the fact that power deposition by the beam, and hence electron density, is usually low near the walls. The return current, though, must be continuous so E_r increases to maintain that continuity. We also find that E_r increases with increasing chamber size, increasing halogen density, and decreasing power deposition. The performance of the laser scales somewhat linearly with the change in the profile of power deposition. Halogen burnup, however, is only weakly dependent on E_r because the rate constant for dissociative attachment decreases while the density of bulk electrons increases, effects which are self compensating. In Section II, we will briefly describe the model we used in this study. The effects of return currents on the performance of fusion class KrF lasers will be discussed in Section III. Concluding remarks are in Section IV.

II. Description of the Model

In this section, the model will be briefly described. The slowing down and deposition of power by the e beam were calculated using a three-dimensional Monte Carlo simulation (MCS). The MCS is essentially the same as described in [8]. It differs in that we collect statistics on the location of where the beam electrons finally stop. We define this location as the point where the beam electrons fall below a specified energy and join the distribution of bulk electrons. This energy was chosen as 100 eV. Below this energy, the mean free path for further energy loss is sufficiently small so that for all practical purposes the beam electron does not move any further. The rate of and location where the beam electrons stop yield the local rate of charge generation, $\dot{\rho}(\vec{r})$ coulombs/(cm^{-3}-s). Results from the MCS additionally provide W values for excitation and ionization (energy/event), and the power, $P(\vec{r})$ [W-cm^{-3}], deposited by beam electrons for use in the plasma chemistry model.

The influx of beam and secondary electrons, $\Phi(\epsilon)$[cm^3-s-eV]$^{-1}$, to the bulk electron distribution is also obtained from the MCS. $\Phi(\epsilon)$ is then used as input to a solution of Boltzmann's equation for the electron energy distribution $f(\epsilon)$. We parameterized the calculation and obtained electron impact rate coefficients as a function of E–N, gas mixture, fractional excitation, and fractional ionization. The rate coefficients were placed into a lookup table for use in the plasma chemistry model. The method of solution of Boltzmann's equation is also described in [8] and is essentially the same as used by Bretagne, *et al.* [11]. The cross sections used for this purpose are also listed in [8].

The electron impact rate coefficients and $\dot{\rho}$ were then used as input to a one-dimensional electron kinetics and plasma chemistry model for an e-beam excited KrF laser. This model is essentially the same as that described in [12] for an electron-beam sustained discharge excited KrF laser. The model contains a full accounting of the pertinent electron impact, ion molecule, excitation transfer, and photo-physics reactions occurring in KrF lasers. The model used here differs from that in [12] in that the electric potential in the plasma is obtained from solution of

$$\nabla \cdot \sigma(\vec{r})\nabla\phi_r(\vec{r}) = \dot{\rho}(\vec{r}) \tag{4}$$

where σ is the plasma conductivity. Equation (4) was solved by the method of successive over relaxation [13] subject to the boundary condition that $\phi_r = 0$ at the grounded chamber walls and $\partial\phi_r/\partial x = 0$ at the center of a symmetrically-pumped plasma. E_r is obtained by differentiating ϕ_r. Electron impact rate coefficients were obtained by consulting the lookup table previously constructed by supplying the instantaneous mole fractions of

the gas species and electrons, and the local value of E_r. Once obtaining ϕ_r, we can use it as input to the MCS to evaluate the change in beam, power and charge deposition resulting from the return current potential.

III. The Effect of Return Currents on Large *E*-Beam Excited KrF Lasers

Our interest in the present paper centers on the effect of return currents on large aperture electron-beam excited KrF lasers, as being developed for inertial confinement fusion, and conceptual designs for larger systems [1], [3], [14]. A model system is the AURORA laser facility at Los Alamos National Laboratory, described in detail in [1]. The AURORA system consists of a chain of laser amplifiers including a front end oscillator, a small aperture module (SAM) (10 × 12 × 100 cm), a power amplifier (PA) (20 × 20 × 300 cm), an intermediate amplifier (IA) (40 × 40 × 300 cm) and a large aperture module (LAM) (100 × 100 × 200 cm). The SAM, PA, and IA are pumped from one side of the chamber. The LAM is symmetrically pumped from both sides. The LAM has delivered in excess of 10 kJ configured as an unstable resonator. Its specifications form the basis of our reference device for this study.

A. Double-Sided Pumping

In this section, we will discuss the effects of return currents in large aperture *e*-beam excited KrF lasers which are symmetrically pumped from both sides of the chamber. Single-sided pumping will be discussed in the following subsection. *E*-beam power deposition and the deposition of charge as a function of position is shown in Fig. 1 for the LAM using single-sided and double-sided pumping (the usual configuration). The *e*-beam voltage is 650 keV, gas pressure is 1350 torr and the gas mixture is Ar–Kr–F_2 = 0.94–0.05–0.005. Although the LAM is usually operated at lower pressures ($\approx$700 torr) there is only a weak pressure dependence of return currents on pressure due to the inherent scaling on *E*–*N* (see discussion below). Note that there is no direct correlation between the spatial distribution of power deposition and of charge deposition. With double-sided pumping, the power deposition is fairly uniform as a function of position except near the foil, however the space charge is deposited with a profile suggesting its loss is dominated by diffusion. This is more clearly shown in the profiles for single-sided pumping. The power deposition is peaked close to the foil and falls off as the beam is depleted. The charge is deposited with a profile which closely resembles that for double-sided pumping. These profiles for power and space charge deposition will be used in the following examples unless noted otherwise. The rise time of the current pulse in these examples is 100 ns, and is constant until 400 ns, falling to zero in another 100 ns. Results are shown for t = 200 ns unless noted, which are quasi-steady-state values.

The fraction of the total power deposition in the LAM which results from the return current heating γ is shown

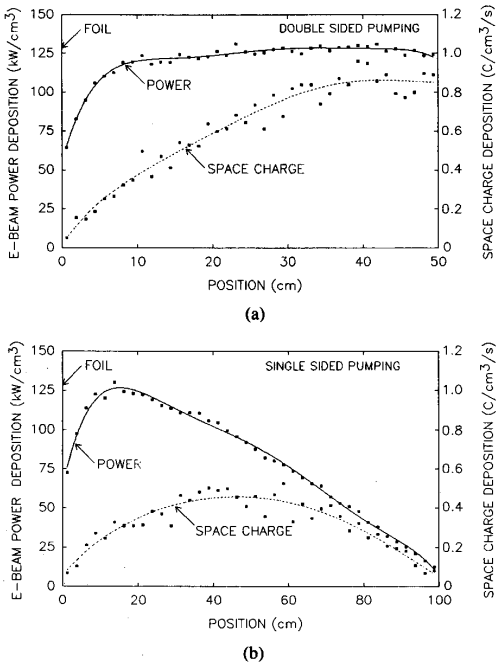

Fig. 1. Typical deposition of power and charge in an *e*-beam excited KrF fusion class laser. The aperture is L = 100 cm. These results were obtained with a Monte Carlo simulation. The squares show the statistical scatter. (a) "Double-sided" pumping by *e* beams from opposite walls. The deposition is therefore uniform over the midplane of the chamber. (b) Single-sided pumping.

as a function of position in Fig. 2(a) for double sided pumping. The gas mixtures are Ar–Kr–F_2 = 0.94–0.05–X, X = 0.0025, 0.005, 0.01 at a total pressure of 1.75 atm. The *e*-beam power deposition is shown for reference and has a maximum value of 132 kW/cm^{-3}. The results are symmetric across the midplane so only half of the chamber is shown. $\gamma(x)$ is zero on the midplane where, by symmetry, E_r = 0. $\gamma(x)$ increases as one approaches the foil, and increases with increasing F_2 density, reaching a maximum fractional value of $\simeq$ 6%. The increase in γ when approaching the foil results primarily from two causes. The first is the decrease in the *e*-beam power deposition, and hence electron density near the foil, which then requires a higher electric field to drive the return current. The second is from the need to drive an increasing amount of return current from the volume as one integrates the deposition of charge from the midplane to the foil.

The normalized return current field, $E_r(x)$–N, and plasma potential $\phi(x)$ are shown in Fig. 2(b) for the same conditions as above. E_r–N exceeds a few Td near the foil, values typically associated with electric discharge lasers. *E*-beam excited lasers operating with these conditions can, in a sense, be described as *e*-beam sustained discharges. The space charge generated potential has a maximum value as high as 18 kV. As this value is small compared to the maximum beam voltage (650 keV), the decelerat-

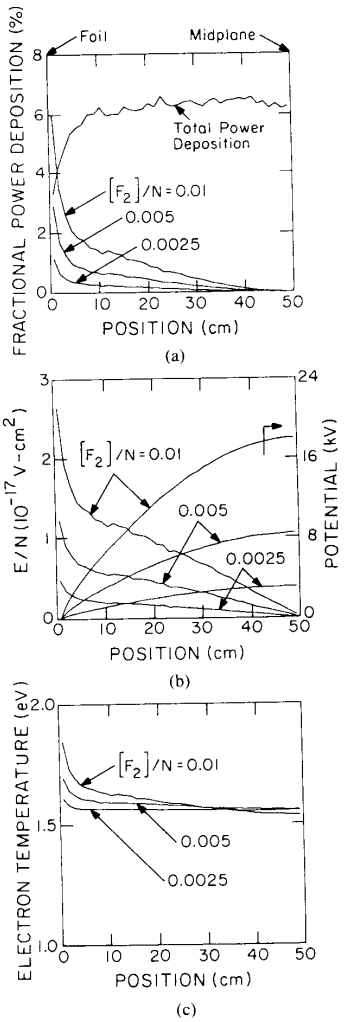

Fig. 2. Pumping parameters for a 1 m aperture electron beam excited KrF laser. The laser has double-sided pumping, the gas pressure is 1.75 atm and results are shown for gas mixtures of Ar-Kr-F_2 = 0.94-0.05-X, X = 0.0025, 0.005, 0.01. The spatial dimension is distance from the e-beam foil located at $x = 0$. The noise in the figures results from the scatter of the Monte Carlo method used to obtain power deposition. (a) Power deposition by the e beam and fraction of total power deposition resulting from the return currents. (b) E_r-N (return current electric field-gas density) and plasma potential. (c) Bulk electron temperature. Due to the decrease in bulk electron density at higher F_2 mole fractions, a larger E_r is required to return the current. This results in higher T_e and more power deposited by the return current field.

ing effect on beam transport is not dramatic. Beam electrons which penetrate only as far as the midplane, where $|\phi_r(x)|$ is a maximum, are decelerated. Those beam electrons which survive to penetrate beyond the midplane, however, are accelerated by the return field, now pointing in the direction of their net transport.

The bulk electron temperature T_e is shown in Fig. 2(c) as a function of position for the same conditions as above. (For non-Maxwellian plasmas, we define $T_e = \frac{2}{3} \cdot \langle \epsilon \rangle$.) Heating of the bulk electron distribution by the return current field increases the electron temperature by as much as 20–25% from its nominal value of 1.5 eV. The fractional change in power deposition, however, is much smaller than the increase in electron temperature. This results from the fact that power deposition is still dominated by the slowing of beam electrons, and not by return current heating. The increase in E_r causes a change in the electron energy distribution (EED) near the foil relative to the center of the chamber. The EED at these two locations are shown in Fig. 3(a). Due to this change in the EED, rate constants for electron impact processes by bulk electrons also change. Low threshold processes, such as dissociative attachment to F_2 and dissociative recombination, have rate constants which decrease near the foil, as shown in Fig. 3(b). Higher threshold processes, such as ionization of the rare gas metastables, have rate constants which increase near the foil.

The differences in electron density n_e and laser intensity I caused by the return currents are shown in Fig. 4. The conditions are the same as in Fig. 2. The maximum power deposition in each case is $\simeq 130$ kW-cm^{-3}. These results compare cases where the return currents are included and ignored in the calculation. The quantity plotted is, for example, $(I(x) - I_0(x))/I_0(x)$, where the subscript denotes the case without including the effects of return currents. The electron densities at the midplane are 2.3×10^{14} cm^{-3}, 8.4×10^{13} cm^{-3}, and 3.9×10^{13} cm^{-3} in increasing order of F_2 fraction (Ar-Kr-F_2 = 0.94-0.05-X, X = 0.0025, 0.005, 0.01). The electron density increases by as much as 5–30% near the foil, albeit in a region of low electron density, as shown in Fig. 4(b). The increase in bulk electron density near the foil results from two factors. The first is that some additional amount of ionization results from the increase in T_e in that region, primarily from collisions with metastable Ar and Kr atoms (e.g., $e + \mathrm{Kr}(5s) \rightarrow \mathrm{Kr}^+ + 2e$). The rate constants for these processes increase near the foil as shown in Fig. 3(b). The second cause is that the rate constant for dissociative attachment of electrons to F_2, the dominant electron loss mechanism, is a decreasing function of E-N. Therefore as E_r-N increases near the foil, the rate constant for attachment decreases. [See Fig. 3(b).] The rate constant for dissociative recombination of dimer ions, the secondary source of electron loss, also decreases with increasing electron temperature ($\sim T_e^{-0.5}$) near the foils. The combined effect is that the electron density increases.

The spatially dependent change in laser intensity is similar in shape, but smaller in magnitude, than that for the electron density, as shown in Fig. 4(c). The increase in laser intensity near the wall results from a real increase in the rate constants for ionization by electron impact processes. This portion of the increase in electron density leads directly to Kr^+, a reactant in the ion–ion neutralization which forms the upper laser level (e.g., $Kr^+ + F^- + M \rightarrow KrF(B) + M$). The difference between the relative increase in the electron density and in laser intensity indicates how much of the increase in electron density

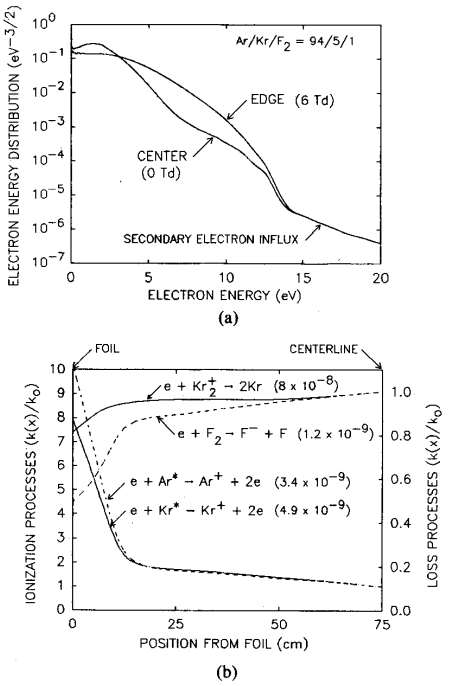

Fig. 3. The effects of E_r on (a) electron energy distributions and (b) electron impact rate constants as a function of position in the laser chamber normalized by their values at the center of the chamber. The values in parenthesis are the rate coefficients ($cm^3 - s^{-1}$) at the center of the chamber. The gas mixture is Ar-Kr-F_2 = 0.94-0.05-0.01. E_r-N = 6 Td at the edge of the chamber.

results from a decrease in the rate constant for electron loss (attachment and recombination), as opposed to an increase in the rate constants for ionization. Any increase in electron density resulting from a decrease in the rate of losses does not result in an increase in the rate of production of precursors to the upper laser. The increase can, however, result in additional electron collision quenching of the upper laser level (e + KrF(B) → Kr + F + e), thereby depressing the laser intensity.

The dependencies of fractional power deposition by the return current $\gamma(x)$ and the local electric potential $\phi_r(x)$ are shown in Fig. 5 as a function of e-beam power deposition. These values were obtained by changing the beam current so that the spatial dependence of power deposition by the beam is essentially unchanged. The cases in Fig. 5 are for maximum power deposition of 65, 130, and 260 kW-cm^{-3}. The times these profiles represent are slightly different to account for differences in the rate of burnup of F_2 resulting from the different power depositions. The scaling law discussed in the introduction (3) implies that the magnitude of the return current should be independent of power deposition. This results from the assumptions that the rate of ionization is directly proportional to power deposition by the beam, and that the electron loss is solely by attachment. The implication is that

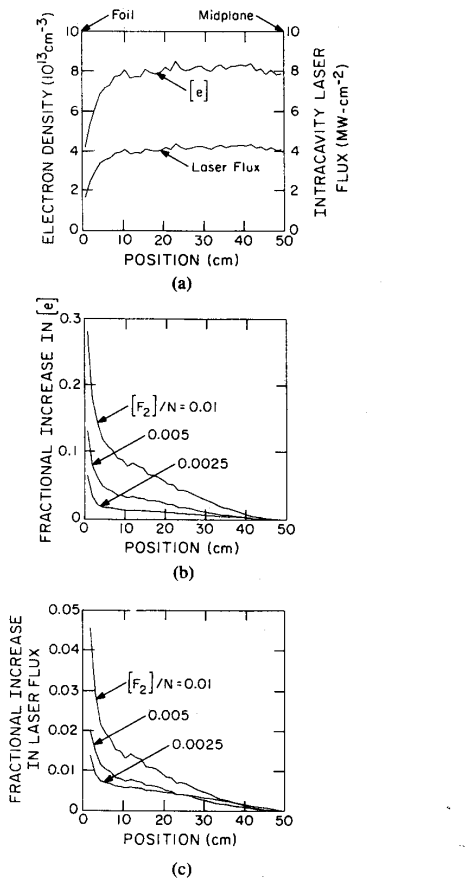

Fig. 4. Dependence of electron density and intracavity laser flux on halogen density and position from the foil. The conditions are the same as in Fig. 2. (a) Spatial distribution of electron density and intracavity laser flux for $[F_2]/N$ = 0.005. (b) Fractional increase in the electron density caused by the return current field compared to the case where the return current fields are not included in the calculation. (c) Fractional increase in the laser flux caused by the return current fields.

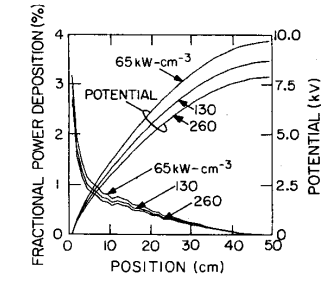

Fig. 5. Fractional power deposition by the return current fields and plasma potential as a function of position for average power depositions of 65, 130, and 260 kW/cm^{-3}. The gas mixture is Ar-Kr-F_2 = 0.94-0.05-0.005. The conditions are otherwise the same as for Fig. 2. There is a weak scaling of fractional power deposition by the return currents on total power deposition. This results from the fact that the electron density with power deposition increases faster than linearly due to the contributions of multistep processes.

increasing power deposition linearly increases the rate of deposition of charge, but also increases the conductivity of the bulk plasma by the same relative amount, so these effects compensate each other. There is, however, a weak scaling of the effects of return currents on power deposition. As shown in Fig. 5, large return current electric fields are obtained at lower power deposition. This is shown by the larger amount of fractional power resulting from E_r and larger plasma potential obtained at lower power deposition. This behavior results from the fact that the *effective* W value (energy-ion pair) of the plasma decreases with increasing power deposition below that value given by the slowing of the e beam alone. This is a result of the increase in ionization obtained from multistep electron impact processes (see above). The conductivity of the bulk plasma therefore increases at a faster rate with increasing power deposition than does the deposition of charge. The electric field required to drive the return current is therefore smaller.

Our simple scaling [(3)] also implies that the effects of the return current fields should increase with increasing aperture size since the volume integrated charge which must be returned to ground increases. Therefore a higher E_r is required to drive the larger current if the conductivity is not changed. The effects of the size of the aperture on laser parameters are shown in Fig. 6, where results are plotted for L = 75, 100, and 150 cm. The conditions for these cases are otherwise the same as in Fig. 1 using the Ar-Kr-F_2 = 0.94-0.05-0.01 mixture. To eliminate the effects associated with differences in the spatial distribution of power deposition, $P(x/L)$ is the same in each case with a maximum value of 130 kW-cm^{-3}. The normalized return current field, $E_r(x)/N$, and plasma potential $\phi_r(x)$ reach 4-5 Td and 40 kV in the large aperture laser (L = 150 cm) as shown in Fig. 6(a). These values are <1.5 Td and <5 kV in the small aperture laser (L = 75 cm). The electric fields cause proportional changes in the electron temperature and in the fractional power deposition by the return currents, as shown in Fig. 6(b). The temperature of the bulk electron distribution is raised by only 0.1 eV near the foil for the small aperture laser, and the fractional power due to the return currents is less $\leq$1-2%. The effect increases with increasing aperture size at a greater than linear rate. The heating near the foil for the large aperture (L = 150 cm) increases the electron temperature to >2 eV and accounts for >12% of the power deposition.

The spatial distributions of the relative changes in electron density and laser intensity scale similarly with aperture size, as shown in Fig. 7. In the large aperture laser, the electron density increases by 45-50% near the foil as a result of the return currents compared to the case where the return currents are ignored, as shown in Fig. 7(a). More than half of this increase is due to a decrease in the rate coefficients for attachment and dissociative recombination resulting from the increase in electron temperature. The remainder is due to more efficient ionization due

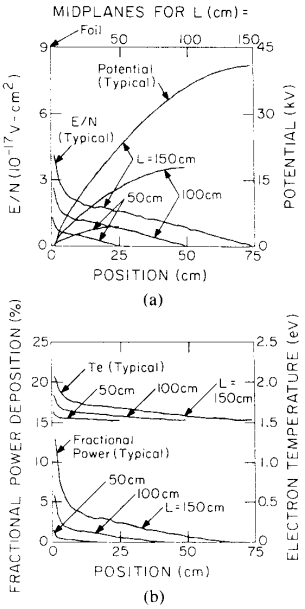

Fig. 6. Plasma parameters as a function of position from the e-beam foil for three different aperture sizes: L = 50, 100, and 150 cm. The same spatial distribution of power deposition by the e beam, $P(x/L)$, was used for each case. (a) E_r-N and plasma potential. (b) Fractional power deposition by the return current fields and bulk electron temperature. Due to the necessity for the return current field to drive the spatially integrated injected current, E_r-N increases with increasing aperture size.

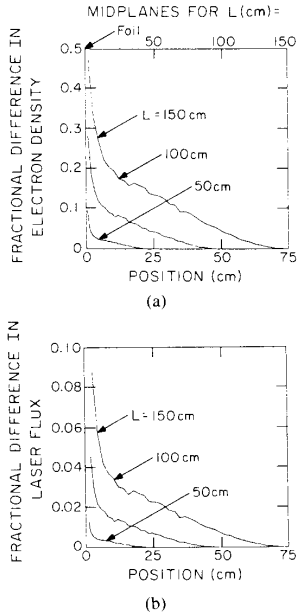

Fig. 7. Fractional increases caused by the return currents in (a) electron density and (b) laser flux as a function of position from the foil. Cases are shown for aperture sizes of L = 50, 100, and 150 cm. The conditions are the same as for Fig. 6.

to multistep processes. The relative increase in laser intensity, though is smaller than the change in electron density, an effect discussed above. The laser intensity increases by only 8–10% near the foil in the larger aperture laser, as shown in Fig. 7(b). The increase in laser intensity is due to the more efficient ionization which occurs from the multistep processes. This increase in efficiency results in a small real increase in the total laser energy (2–5%) obtained from the system.

In spite of these large changes in electron density and rate coefficients resulting from E_r, the change in the burnup of F_2 is only nominal in all cases (a few percent more burnup near the foil). This results from the fact that E_r causes a decrease in the rate constant for dissociative attachment, and an increase in the density of bulk electrons, which are self-compensating.

To determine the effects of the return currents at different gas pressures under "realistic" conditions, we varied the gas pressure, *e*-beam voltage and *e*-beam current so that the spatial distribution of power deposition was approximately the same. The resulting power deposition profiles are shown in Fig. 8(a) for 1 atm (V_b = 450 kV), 1.75 atm (V_b = 600 kV), and 3 atm (V_b = 900 kV) for L = 100 cm. The electron temperature and return current field are shown in Fig. 8(b). There are only nominal differences between these cases, with T_e and E_r increasing in magnitude with increasing pressure. This effect is due to the decrease in electron density obtained at the higher pressures, shown in Fig. 8(c). The decrease in n_e results from the faster rate of ion dimerization, followed by rapid dissociative recombination, which occurs at higher gas pressures.

There is interest in using Ar–Kr–F_2 gas mixtures having high concentrations of Kr (10–100%) due to improvements in laser efficiency that may result [4], [15]. To investigate this parameter space we repeated the previous calculations for Kr concentrations of 10 and 30%, which bracket the optimum concentration in terms of laser energy efficiency [15]. When keeping the power deposition and pressure a constant, we found only a small influence of Kr concentration on the return current electric field. E_r increases only a few percent over the range of Kr concentrations studied (5–30%). One would expect that increasing the Kr concentration would also increase E_r since the cross section for electron momentum transfer to Kr is larger than that for Ar. The W value for ionization by beam electrons though decreases as the fraction of Kr increases. Therefore with a fixed power deposition, the rate of ionization, and hence electron density, increases. The increase in electron density and rate of momentum transfer experienced with increasing Kr fraction are compensating effects which result in keeping the conductivity of the plasma nearly constant. As a consequence, E_r does not have a strong dependence on Kr concentration.

B. Single-Sided Pumping

Based on our previous discussion, one would expect that return currents will have a greater impact on large aperture *e*-beam excited lasers which are pumped from only one side, as compared to double-sided pumped systems. This expectation results from the fact that in single-sided pumped systems there is usually a weakly excited region near the opposite wall from the foil. In this volume, the local charge deposition may not by proportionally small [see Fig. 1(a)]. To investigate the effects of return currents on the characteristics of large aperture *e*-beam excited plasmas using single sided excitation, we used the power and deposition profiles shown in Fig. 1(b). This study may be considered something of a worst case since the nonuniformity of the power deposition shown in Fig. 1(b) is somewhat severe. This degree of nonuniformity, though, is unavoidable if one desires to stop the *e* beam and deposit all of its power in the gas. By operating with a gas pressure and mixture which has a lower stopping power, the beam will more uniformly deposit power in

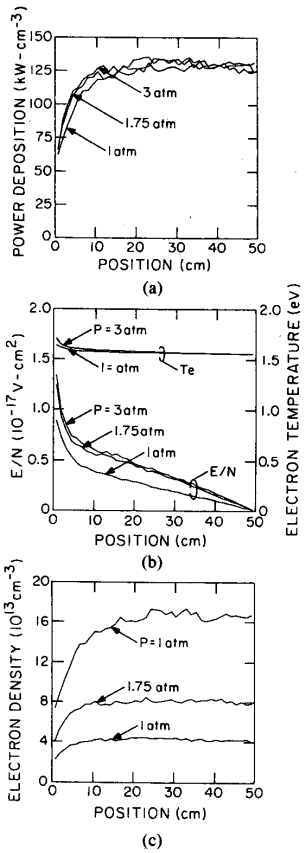

Fig. 8. Plasma parameters as a function of position from the *e*-beam foil for gas pressures of 1 atm (V = 450 keV), 1.75 atm (V = 600 kV), and 3.0 atm (V_b = 900 keV). The *e*-beam voltages and currents were selected in each case to result in approximately the same power deposition by the beam. The gas mixture is Ar–Kr–F_2 = 0.94–0.05–0.005. (a) Power deposition by the *e* beam. (b) Return current electric field (E–N) and electron temperature. (c) Electron density. There is a weak scaling of the return current electric field on gas pressure due to the higher rate of recombination that occurs at higher pressures.

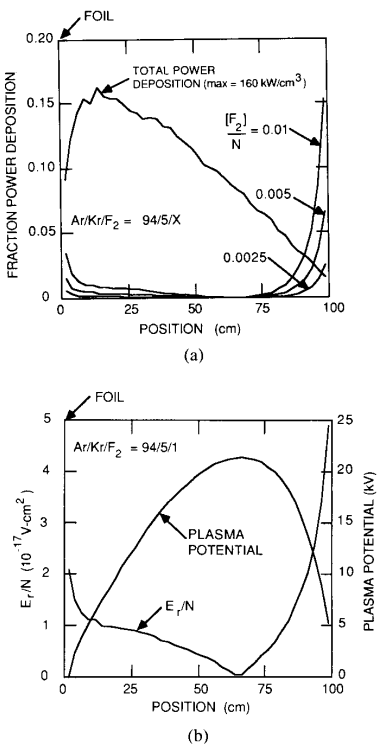

Fig. 9. Plasma parameters for the LAM using single-sided pumping. The beam enters through the foil at $x = 0$. The gas mixture is Ar-Kr-F_2 = 0.94-0.05-X, X = 0.0025, 0.005, and 01 at 1.75 atm. (a) Fractional power deposition by the return currents, and total power deposition. (b) E_r/N and plasma potential for $[F_2]/N = 0.01$.

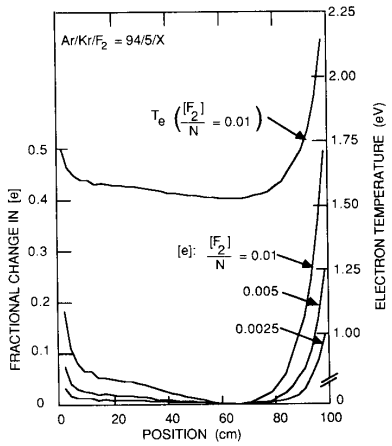

Fig. 10. Fractional change in electron density and electron temperature for single sided pumping of the LAM. The conditions are the same as in Fig. 9. The fractional increase in electron density is >0.45 in the poorly pumped region near the far wall where the electron temperature increases by ≈0.76 eV.

the gas, but it will also traverse the chamber and strike the opposite wall.

Fractional power deposition resulting from the return current for the standard LAM conditions (1.75 atm, Ar-Kr-F_2 = 0.94-0.05-X, X = 0.0025, 0.005, 0.01) using single-sided pumping is shown in Fig. 9(a). For reference, the profile of power deposition by the e beam alone is also shown in the figure. The maximum power deposition near the foil is 160 kW-cm^{-3}. Greater than 0.15 of the power deposition near the far wall results from the return currents for the case with high halogen fraction, albeit in a region of low total power deposition. E_r-N is ≈5 Td in this region and the maximum plasma potential is in excess of 20 kV. Note that the peak in the plasma potential is offset from the centerline and occurs far from the maximum in power deposition.

The increase in E_r-N near the far wall results in an increase in the rate coefficients for ionization, and reductions in the rate coefficients for electron loss by dissociative attachment and recombination. The result is a large fractional increases in electron density near the far wall, as shown in Fig. 10. The electron density in the absence of the return currents is nearly linearly proportional to the local power deposition, with maximum values of 3.0×10^{14}, 1.1×10^{14} and 4.3×10^{13} cm^{-3} for $[F_2]/N$ = 0.0025, 0.005, and 0.01, respectively. The fractional increase in electron density near the far wall exceeds 0.45 for $[F_2]/N = 0.01$. The increase in electron temperature in this volume is nearly 0.75 eV. The large fractional increases in power deposition and electron density resulting from the return currents, and the high E_r-N near the far wall leads one to suggest that large aperture e-beam excited lasers functionally operate as e beam sustained discharges in volumes which are poorly pumped by the beam.

IV. Concluding Remarks

The effects of return currents and electric fields have been studied in large aperture ($L > 75$ cm) electron beam excited KrF lasers. The joule heating resulting from the return current redistributes power into regions which are weakly pumped by the e-beam electrons, such as near the foil in double-sided pumped systems and near the far wall in single-sided pumped systems. The return current electric field in these regions may be a few to 10 Td in the large apertures ($L \approx 150$ cm). The result is that the bulk electron distribution is heated, raising the electron temperature by as much as 0.5–1.0 eV. The higher bulk electron temperature has two important effects. The first is that the rate constants for dissociative attachment of electrons to F_2 and for dissociative recombination decrease. The second is that the rate constants for multistep electron impact ionization of rare gas metastable atoms increases. Ionization by the latter process is highly efficient compared to ionization by beam electrons. The result is that the bulk electron density increases in those regions weakly pumped by the beam and laser power increases. Due to the more efficient ionization caused by the return currents, there may be a real, but small (<5%) increase in the total laser energy as a result of the return current fields. The dominant effect, though, is to redistribute the power dep-

osition, and hence laser power, to a more uniform spatial distribution.

The effects of the return currents increase with increasing F_2 fraction, increasing aperture size, increasing gas pressure, decreasing power deposition, and increasing nonuniformity of power deposition by the beam. The effects, however, are only important in large aperture lasers. Large aperture lasers having poorly-pumped volumes functionally operate as *e*-beam sustained discharges. These effects should be considered in the analysis of fusion class lasers having apertures >75–100 cm, but may be ignored in conventional lasers having apertures <10's cm.

Acknowledgment

The author would like to thank D. E. Hanson and D. Cartwright of Los Alamos National Laboratory and J. Jacob of Science Research Laboratories for their comments and direction.

References

[1] L. A. Rosocha, J. A. Hanlon, M. McLeod, M. Kang, B. L. Kortegaard, M. D. Burrows, and P. S. Bowling, "AURORA multikilojoule KrF laser system prototype for inertial confinement fusion," *Fusion Technol.*, vol. 11, pp. 497–531, 1987.

[2] A. Endoh, M. Watanabe, N. Sarukura, and S. Watanabe, "Multiterawatt subpicosecond KrF laser," *Opt. Lett.*, vol. 353–355, 1989.

[3] A. M. Hunter, R. O. Hunter, Jr., and T. H. Johnson, "Scaling of KrF lasers for inertial confinement fusion," *IEEE J. Quantum Electron.*, vol. QE-22, pp. 386–404, 1986.

[4] F. Kannari, M. J. Shaw, and F. O'Neill, "Parametric studies of an electron beam pumped krypton rich KrF laser," *J. Appl. Phys.*, vol. 61, pp. 476–488, 1987.

[5] J. Goldhar and L. G. Schlitt, "RAPIER experiments," in *1981 Laser Program Annual Report* E. V. George Ed. Livermore, CA: Lawrence Livermore Nat. Lab., 1982, pp. 7-82–7-94.

[6] J. A. Mangano, J. Hsia, J. H. Jacob, and B. N. Strivastava, "Plasma return current discharge," *Appl. Phys. Lett.*, vol. 33, pp. 487–489, 1978.

[7] The *W* value is the amount of energy which must be deposited in the gas to produce a particular excited state of the gas, in this case an ion. The *W* value is typically larger than the ionization potential due to the loss of energy to other excitation channels. See [8].

[8] M. J. Kushner, "Response times and energy partitioning in electron beam excited plasmas," *J. Appl. Phys.*, vol. 66, pp. 2297–2306, 1989.

[9] B. E. Cherrington, *Gaseous Electronics and Gas Lasers*. Oxford: Pergammon, 1979, ch. 4.

[10] H. T. Powell, private communication, 1990.

[11] J. Bretagne, J. Godart, and V. Puech, "Low energy electron distribution in an electron-beam generated argon plasma," *J. Phys. D*, vol. 15, pp. 2205–2225, 1982.

[12] M. J. Kushner and A. L. Pindroh, "Discharge constriction, photodetachment and ionization instabilities in electron-beam-sustained discharge excimer lasers," *J. Appl. Phys.*, vol. 60, pp. 904–914, 1986.

[13] W. F. Ames, *Numerical Methods for Partial Differential Equations, 2nd ed.* New York: Academic, 1977, pp. 114–135.

[14] D. L. Lowenthal, J. J. Ewing, R. E. Center, P. B. Mumola, W. G. Grossman, N. T. Olson, and P. J. Shannon, "Conceptual design of an angularly multiplexed 50 kJ KrF laser for ICF," *IEEE J. Quantum Electron.*, vol. QE-17, pp. 1861–1870, 1981.

[15] E. T. Salesky and W. D. Kimura, "Electron-beam pumped KrF laser extraction measurements for high Kr concentration gas mixtures," *IEEE J. Quantum Electron.*, vol. QE-21, pp. 1761–1765, 1985.

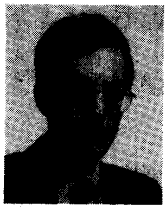

Mark J. Kushner (S'78–M'79–SM'89), was born in Los Angeles, CA on December 21, 1952. He received the B.A. degree in astronomy and the B.S. degree in Engineering from the University of California, Los Angeles in 1976 and the M.S. and Ph.D. degrees, both in applied physics, from the California Institute of Technology, Pasadena in 1977 and 1979, respectively. While at Caltech he also held the position of Chaim Weizmann Postdoctoral Research Fellow.

Dr. Kushner served on the technical staffs of Sandia National Laboratory and Lawrence Livermore National Laboratory before joining Spectra Technology (formerly Mathematical Sciences Northwest). At Spectra Technology, he was a Principal Research Scientist and Director of Electron, Atomic, and Molecular Physics. In August 1986, he joined the Department of Electrical and Computer Engineering at the University of Illinois, (Urbana-Champaign), where he currently holds the rank of Associate Professor. He has published 65 refereed papers and presented more than 120 conference papers on topic related to gas and solid-state lasers, pulse-power plasmas, plasma processing, chemical lasers, and laser spectroscopy. His work now primarily involves developing continuum and Monte Carlo particle computer simulations for gas discharges, low-temperature plasmas and the growth of amorphous materials.

Dr. Kushner is a member of Phi Beta Kappa, Tau Beta Pi, Sigma Xi, the American Physical Society, the Optical Society of America, and the Materials Research Society.